Borrelia and *Chlamydia* Can Form Mixed Biofilms in Infected Human Skin Tissues

E. Sapi[1*], K. Gupta[1], K. Wawrzeniak[1], G. Gaur[1], J. Torres[1], K. Filush[1], A. Melillo[1] and B. Zelger[2]

[1]*Department of Biology and Environmental Science, University of New Haven, West Haven, CT 06516, USA*
[2]*Department of Dermatology and Venereology, Medical University Innsbruck, Innsbruck, Austria*

Received: 15 January 2019; accepted: 04 March 2019

Our research group has recently shown that *Borrelia burgdorferi*, the Lyme disease bacterium, is capable of forming biofilms in *Borrelia*-infected human skin lesions called *Borrelia* lymphocytoma (BL). Biofilm structures often contain multiple organisms in a symbiotic relationship, with the goal of providing shelter from environmental stressors such as antimicrobial agents. Because multiple co-infections are common in Lyme disease, the main questions of this study were whether BL tissues contained other pathogenic species and/or whether there is any co-existence with *Borrelia* biofilms. Recent reports suggested *Chlamydia*-like organisms in ticks and *Borrelia*-infected human skin tissues; therefore, *Chlamydia*-specific polymerase chain reaction (PCR) analyses were performed in *Borrelia*-positive BL tissues. Analyses of the sequence of the positive PCR bands revealed that *Chlamydia* spp. DNAs are indeed present in these tissues, and their sequences have the best identity match to *Chlamydophila pneumoniae* and *Chlamydia trachomatis*. Fluorescent immunohistochemical and in situ hybridization methods demonstrated the presence of *Chlamydia* antigen and DNA in 84% of *Borrelia* biofilms. Confocal microscopy revealed that *Chlamydia* locates in the center of *Borrelia* biofilms, and together, they form a well-organized mixed pathogenic structure. In summary, our study is the first to show *Borrelia–Chlamydia* mixed biofilms in infected human skin tissues, which raises the questions of whether these human pathogens have developed a symbiotic relationship for their mutual survival.

Keywords: Lyme disease, biofilm, *Borrelia* lymphocytoma, alginate, chlamydia, confocal microscopy

Introduction

Lyme disease is a tick-borne illness that is caused by *Borrelia burgdorferi* sensu stricto and sensu lato in the United States and Europe, respectively [1–5]. Lyme disease is estimated to affect 300,000 people a year in the United States and 65,000 people a year in Europe [6]. The most common skin manifestation is a red rash that is observed after a tick bite called erythema migrans (EM) [7, 8]. The other well-studied dermatological conditions of Lyme disease are *Borrelia* lymphocytoma (BL) that appears in the early phase of *Borrelia* infection and acrodermatitis chronica atrophicans (ACA), which is the late onset cutaneous manifestation [9–12]. However, Lyme disease is a multi-systemic disease with manifestations that may also include other several chronic conditions such as Lyme carditis and neuroborreliosis [13–18].

Recently, our research group provided evidence for both the *B. burgdorferi* sensu stricto and the sensu lato groups of *B. burgdorferi* to exist in biofilm form in vitro and in vivo in *Borrelia* lymphocytoma [19–21]. Like other bacterial biofilms, *Borrelia* biofilms have shown increased resistance towards the standard antibiotics that are used to treat Lyme disease [22]. Biofilms are an aggregation of planktonic bacteria that attach on biotic and abiotic surfaces to form a three-dimensional architecture to withstand various environmental stressors [23]. The presence of a protective surface matrix called extracellular polymeric substance (EPS) and persister cells with low metabolic activity helps the survival of community inside the biofilm [24–30]. Clinically, biofilm infections represent a very significant problem due to the extraordinary resistance to both antimicrobial drugs, as well as host immune systems, which eventually could lead to persistent human infections [29, 31–33]. According to the National Institute of Health (NIH), 80% of all chronic infections have been linked to pathogenic biofilms [33, 34]. Several biofilm-related chronic infections have been reported such as *Pseudomonas aeruginosa* in cystic fibrosis [35], *Escherichia coli* in urinary tract infections, *Staphylococcus aureus* in osteomyelitis and endocarditis, and *Streptococcus pneumoniae* in pulmonary infections [33, 36–38].

Highly diverse in nature, biofilms have been reported to exist in a polymicrobial fashion, where several bacterial species along with fungi, yeast, and viruses reside in a community [39, 40]. The microbial community communicates through quorum sensing, co-operates with each other by developing a symbiotic relationship, protects and fights against antimicrobial treatments [39, 40]. The presence of mixed biofilms has been suggested in oral plaques, gastrointestinal tract, chronic wounds, and lungs, enhancing biofilm formation and increasing the resistance against stress and the host immune responses [41–44].

In Lyme disease, co-infections are common because ticks are well known to carry and transmit several human pathogenic microbes along *Borrelia* such as *Bartonella*, *Ehrlichia*, *Babesia*, *Anaplasma*, and even *Mycoplasma* species [45–49]. Recently, the presence of *Chlamydia*-like organisms was also reported by several studies in a significant fraction of *Ixodes ricinus* ticks [50–52]. Furthermore, the presence of *Chlamydia* DNAs in 68% of the skin biopsies obtained from patients with a suspected tick bite history was found [52]. The follow up

*Author for correspondence: 300 Boston Post Road, West Haven CT 06516; Tel.: +1-203-479-4552; E-mail: E-mail: esapi@newhaven.edu.

DOI: 10.1556/1886.2019.00003

study from the same research group reported that all *Borrelia* positive granuloma annulare skin conditions were also positive for *Chlamydia* related bacteria [53]. Furthermore, a recent Australian study also confirmed that DNA from ticks contains DNA belonging to the chlamydial order genotype [54] suggesting that *Chlamydia* can be a very frequent co-infection in *Borrelia* infected tissues.

The bacterial order *Chlamydiales* includes intracellular Gram-negative bacteria that follow a biphasic development cycle and are dependent on the host organism for ATP synthesis [55]. The bacteria primarily exist as elementary bodies capable of invading the host cell [56]. Following infection in the host cell, they fuse with the membrane-bound cytoplasmic vacuole, termed inclusion bodies, where they are in a protective environment [56, 57].

There are 3 main *Chlamydia* pathogens responsible for causing human infections. *Chlamydophila pneumoniae* is a respiratory pathogen whose infection leads to extra-pulmonary symptoms such as myocarditis, atherosclerosis, reactive arthritis, and nervous system disorders [58, 59]. *Chlamydia trachomatis* is a bacterium responsible for causing sexually transmitted diseases such as urethritis, cervicitis, and some other infections, such as Reiter's syndrome, reactive arthritis, ocular infections, atypical pneumoniae, or pelvic inflammatory diseases [60]. *Chlamydia psittaci* is a pathogen that affects avians and is known to cause the human infection psittacosis leading to severe pneumonia [61]. Erythema nodosum, an inflamed skin condition with painful, red deep-seated nodules on lower legs, is also observed after chlamydial infection [62]. Several chlamydial infections have similar symptoms, as observed in Lyme patients such as arthritis, atherosclerosis, neurocognitive symptoms, and skin rashes [45, 63].

Chlamydia-related infections have been reported to be developing an emerging resistance to antibiotics in vitro and in clinical samples [64, 65]. There is no direct evidence for the existence of *Chlamydia* in biofilm form; however, studies have reported the existence of chlamydial aggregates due to stressful conditions such as calcium imbalance [66, 67].

Based on these findings, the goal of this study was to investigate the potential presence of *Chlamydia* spp. in BL skin biopsies and their potential relationship to *Borrelia* biofilms reported previously in BL skin biopsies.

Materials and Methods

Human Skin Sections. From the files of our dermatohistopathologic laboratory, paraffin materials from 6 cases of clinically confirmed *Borrelia* lymphocytoma were archived from January 1975 to December 2005. All six cases had positive serology for *Borrelia* IgG and characteristic features of *Borrelia* lymphocytoma with "acral" predilection were found. All six patients were female (average age = 33 years) from endemic areas of borreliosis in Austria with a rate of positive serology in the population between 30–60%. Polymerase chain reaction (PCR) confirmation for all 6 cases was performed independently in 2 different laboratories located in Austria and the US. The archived hematoxylin-and-eosin (H&E)-stained sections were reexamined, and the previous diagnosis also confirmed. Institutional Review Board exemption for this study was obtained from the University of New Haven. The paraffin blocks were sectioned by McClain Laboratories LLC [Smithtown NY] at 4 μm on TRUBOND200 adhesive slides. The sections then were deparaffinized by washing the sections three times in 100% xylene for 5 min each, followed by rehydration in a series of graded alcohols (100%, 90%, and 70%) and washed in 1× phosphate buffered saline (PBS) of pH 7.4 for 5 min. For the immunohistochemical experiments, the tissues were incubated in 10 mM sodium citrate buffer for 45 min at 95 °C for antibody retrieval.

DNA Extraction. DNA extraction from FFPE samples was performed using the Qiagen Gene Read DNA FFPE Kit (Qiagen, Germantown, MD) according to the manufacturer's handbook with some modifications: 4-μm paraffin-embedded tissue sections were deparaffinized by heating slides for 10 min at 45 °C followed by 3 xylene washes, 5 min each wash. Tissues were then rehydrated in a series of alcohol (100%, 100%, 90%, and 70%) washes for 3 min each. Slides were run under a slow stream of tap water in a container with 70% alcohol for 30 min. Tissue sections were scraped into 1.5-mL tubes using a sterile razor blade; the 56 °C proteinase K digestion step was performed for 72 h; the AW1 and AW2 wash steps were performed three times.

Polymerase Chain Reaction. PCR reactions for *Borrelia burgdorferi* sensu lato were performed on all BL biopsy samples in previous studies by 2 independent laboratories [8, 21], and positive *Borrelia afzelii* DNAs were found on all 6 samples. To detect the specific *Chlamydia* spp. in the skin tissue samples, 2 different previously published PCR methods were used to maximize the probability to amplify *Chlamydia* spp. [68, 69]. Both PCR protocols were designed to detect the Outer Membrane Protein A (OmpA) gene, which was proven to be specific enough to identify the different *Chlamydia* species [68, 69]. Positive control reactions consisted of commercially available DNA samples (not live cultures) from *Chlamydophila pneumoniae* strain CM-1 [ATCC® VR-1360™] and *Chlamydia trachomatis*, both obtained from American Type Culture Collection (ATCC) (Serovar E *Chlamydiaceae* VR 348BD BOUR strain). As negative controls, reactions with no template DNA and normal healthy human DNA samples were used. The first PCR protocol was slightly modified and included an additional pre-amplification of the OpmA DNA in the BL tissues in a nested PCR reaction. In the first round, primers specific to the outer membrane protein A (OmpA) gene were used: forward 5′-CGCATTTGCTGGTTCTGTT-3′ and reverse 5′-CCAACGAGATTGAACGCTGT-3′ primer sequences (Integrated DNA Technologies). In a 25 μL reaction, 1× PCR buffer (Promega), 1.5 mM $MgCl_2$, 0.2 mM dNTPs, 0.2 μM forward primer, 0.2 μM reverse primer, 1.25 U of DNA polymerase, and 50 ng of DNA template were added. Reaction conditions were defined by an initial denaturing time of 95 °C for 5 min, followed by 35 cycles of 95 °C/45 s, 53 °C/15 s, 55.4 °C/15 s, 72 °C/45 s, and a final extension of at 72 °C/5 min. Primers for the nested reaction were as follows: forward 5′-CTCCTTACAAGCCTTGCCTGTAGGG-3′, reverse 5′-GCGATCCCAAATGTTTAAGGC-3′. [68]. A 50 μL nested PCR reaction was prepared by adding 1× Buffer B (Promega, Madison WI), 1.5 mM $MgCl_2$, 0.2 mM dNTPs, 0.2 μM forward primer, 0.2 μM reverse primer, 1.25 U of DNA polymerase, and 1 μL of a 1:100 dilution of the first reaction product. Reaction conditions were defined by an initial denaturing time of 95 °C for 5 min, followed by 35 cycles of 95 °C/60 s, 53.4 °C/30 s, 72 °C/60 s, and a final extension of at 72 °C/5 min. The 337 bp PCR products were analyzed by standard agarose gel electrophoresis, and the PCR products were purified using a QIAquick PCR purification kit (Qiagen, Germantown, MD) according to the manufacturer's instructions. Samples were eluted twice in 30 μL, and the eluates from each sample were pooled and sequenced in both directions twice (4× coverage) using the same primers that generated the products. All DNA sequencing was performed by Eurofins Genomics (Louisville, KY).

In the second PCR protocol, a different published primer pair spanning the major outer membrane protein (OmpA)

region of the *Chlamydia* species was used (69). Primers were forward 5′-CCTGTGGGGAATCCTGCTGAA-3′ and reverse 5′-GTCGAAAACAAAGTCACCATAGTA-3′ flanking a 144 bp region of the gene. For the PCR conditions, a final reaction volume of 50 μL was set with 0.2 mM dNTPs, 2.5 U of Taq DNA polymerase (Invitrogen, Carlsbad CA), 0.2 μM of each forward and reverse primer, 1.5 mM of $MgCl_2$, and 1× Buffer B (Promega, Madison WI). The temperature profile was set for initial denaturation at 94 °C for 4 min, followed by 40 cycles of denaturation at 94 °C for 1 min, annealing at 53 °C for 1 min, and extension at 72 °C for 2 min, followed by a final extension at 72 °C for 5 min. The PCR products were analyzed by standard agarose gel electrophoresis, and the PCR products were purified using the QIAquick PCR purification kit (Qiagen, Germantown, MD) and sequenced as described above.

All resulting sequences were first analyzed using the Basic Local Alignment Search Tool on the NCBI website (BLAST, https://blast.ncbi.nlm.nih.gov/Blast.cgi). The sequences were aligned to reference sequences using the CLUSTEL OMEGA multiple sequence alignment tool (EMBL-EBI, http://www.ebi.ac.uk/Tools/msa/clustalo/).

Immunohistochemistry. Before proceeding with immunostaining, the deparaffinized slides were rinsed with 1× phosphate buffered saline (PBS, Sigma, St. Louise MO) and distilled water for 2 min each. Slides were pre-incubated with 10% normal goat serum (Thermo Scientific) in PBS–0.5% bovine serum albumin (BSA, Sigma) for 30 min at room temperature (RT) to block the nonspecific binding of the secondary antibody. Slides were then rinsed twice with 1× PBS and distilled water for 2 min each at RT. The slides were then treated with a dilution of 1:200 (dilution buffer: PBS pH 7.4 + 0.5% BSA) of monoclonal antibody for *Chlamydia* spp. (Cat# C65815M, Meridian Life Sciences, USA) and incubated overnight in a humidified chamber at 4 °C. The slides then were washed in 1× PBS and distilled water five times for 2 min each at RT. The tissue sections were then incubated with a 1:200 dilution of the secondary anti-mouse antibody (dilution buffer: PBS pH 7.4 + 0.5% BSA) with a fluorescent red tag (goat anti-mouse IgG (H+L), DyLight 594 conjugated for an hour at RT in a humidified chamber. The excess solution around the tissue was gently wiped, washed five times as mentioned above with 1× PBS, and then, the polyclonal rabbit anti-alginate antibody (generously provided by Dr. Gerald Pier, Harvard Medical School) was diluted in a 1:500 ratio (dilution buffer: PBS pH 7.4 + 0.5% BSA) and added to the slides. The slides were incubated at RT overnight in a humidified chamber. The next day the slides were washed five times with 1× PBS for 2 min each. The tissue sections were then treated with a 1:200 dilution (dilution buffer: PBS pH 7.4 + 0.5% BSA) of the secondary anti-rabbit antibody with a fluorescent blue tag (goat anti-rabbit IgG (H+L), DyLight 405 conjugated) and incubated for an hour. This step was followed by the abovementioned washes and then treatment with a 1:50 dilution of a fluorescein isothiocyanate (FITC)-labeled polyclonal rabbit anti-*Borrelia burgdorferi* antibody (PA-1-73005, Thermo scientific), for an hour in a humidified chamber at room temperature. The slide sections were then washed and processed as mentioned above and then counterstained with 0.1% Sudan black (Sigma) for 20 min, washed again, and then mounted with PermaFluor (Thermo Scientific). Images were taken and processed using a Leica DM2500 fluorescence microscope at 200× and 400× magnification.

As negative controls, commercially available human newborn foreskin tissue sections and healthy human skin sections (Biomax, HuFPT136) were stained following the same procedure as mentioned above. Additional negative controls such as omitting the primary antibody and the use of non-specific isotype IgG controls (IgG1 Isotype Control, Invitrogen, MA1-10406) were also utilized to confirm the specificity of the antibodies.

Fluorescent in situ Hybridization (FISH). The paraffin-embedded tissue sections were deparaffinized and hydrated in a series of alcohol washes as mentioned above. The tissue sections were then placed in a solution of sodium borohydride for 20 min on ice. Tissues were fixed with 4% paraformaldehyde (PFA, J.T Baker) for 15 min at RT. Next, the sections were washed with 2× saline sodium citrate (SSC) buffer for 5 min and digested with 100 ug/mL of proteinase K (Sigma) at RT for 15 min. The slides were then treated with denaturing solution (70% *v/v* formamide and 2× SSC) and incubated for 5 min at 95 °C and at RT. The slides were fixed again with 4% PFA for 10 min at RT and washed with 2× SSC before being again placed in denaturing solution at 60 °C for 2 min. The salmon sperm DNA (2.5 ng, Thermo Fisher Scientific) was prewarmed at 95 °C for 5 min and added to the slides for blocking for an hour at 48 °C. The slides were then incubated with previously validated fluorescent in situ DNA probes [21, 70]: *Borrelia*-specific 16S rDNA probe (FAM-5′-GGATATAGTTAGAGATAATTATTCCCCGTTTG-3′) and *Chlamydia*-specific 16S rDNA probe (Alexa 568 5′-CCTCCGTATTACCGCAGC-3′) after denaturing the probes at 95 °C for 10 min. A coverslip was placed on the slide to ensure that the tissue did not dry out, and the tissue sections were incubated for 16 h overnight at 48 °C. After overnight incubation, the coverslip was removed by placing the slides in 2× SSC for 5 min, followed by five-time washes of 0.2× SSC buffer for 5 min each at RT in the dark. Sections were then counterstained with 0.1% Sudan black dye (Sigma) for 20 min in the dark at RT. The slides were washed five times with 2× SSC for 5 min before mounting the slides with PermaFluor mounting media (Thermo Scientific) and stored at 4 °C. Images were taken using a Leica DM2500 fluorescence microscope at 200× and 400× magnification.

All FISH steps were repeated with several negative controls such as the following: 1) 100 ng random oligonucleotide, (5′-FAM-GCATAGCTCTATGACTCTATACTGGTACGTAG-3′), 2) 200 ng of unlabeled competing oligonucleotide added before the hybridization step [competing *Borrelia* (5′-CAAACGGGGAATAATTATCTCTAACTATATCC-3′) and competing *Chlamydia* (5′-CCTCCGTATTACCGCGGC-3′)], and 3) a DNase treatment of the sections before the hybridization step to digest all genomic DNA (100 μg/mL for 60 min at 37 °C).

A combination of immuno and in situ protocols was performed in a similar fashion as described earlier [21]. Briefly, after the 0.2× SSC wash in the FISH protocol the sections were blocked with a 1:200 dilution of goat serum (Thermo Scientific) for an hour at RT in a humidified chamber. The slides were washed five times with PBS followed by adding the primary polyclonal anti-alginate antibody for overnight incubation at RT. The next day the slides were tagged with a 1:200 dilution of the secondary anti-rabbit antibody with a fluorescent blue tag (goat anti-rabbit IgG (H+L), DyLight 405 conjugated) and incubated for an hour at RT. This step was then followed by a counterstaining step with 0.1% Sudan black for 20 min, followed by several washes in 0.2× SSC and mounting with PermaFluor mounting media (Thermo Scientific) and storing at 4 °C. Images were taken using Leica DM2500 fluorescent microscope at 200× and 400× magnification.

Confocal Microscopy. The tissue sections were visualized and scanned with a confocal scanning laser microscope (Leica

DMI6000) for generating *z*-axis stacks for visualization of the dual species biofilm in a three-dimensional view. ImageJ software was used to process the generated *z* stacks in order to receive a detailed analysis of the spatial distribution of the multi-species biofilms (Plugins: Interactive 3D Surface Plot and Volume Viewer).

Ethics. The study used archived paraffin embedded sections which was sent to University of New Haven without any identification. The Institutional Review Board at the University of New Haven approved the study under 45 CFR 46.101(b)(4): Research involving the collection or study of existing data, documents, records, pathological specimens, or diagnostic specimens, if these sources are publicly available or if the information is recorded by the investigator in such a manner that subjects cannot be identified, directly or through identifiers linked to the subjects.

Results

PCR Analyses of *Borrelia*-Positive BL Skin Tissues for *Chlamydia* spp.. The first aim of the study was to evaluate the potential presence of *Chlamydia* spp. in the *Borrelia*-positive biopsy tissues of BL patients. We used archived skin biopsies from our previous studies, in which we proved that the BL tissues are positive for *Borrelia afzelii* DNA using PCR methods performed by two independent research laboratories previously [8, 21]. To amplify *Chlamydia* spp. DNA, several previously published PCR protocols were utilized which were designed to amplify the major outer membrane protein A (OmpA) gene and were able to identify the species [68, 69]. The *Chlamydia* OmpA-specific PCR protocols resulted in positive bands in the BL tissues studied. Interestingly, when the DNAs were sequenced and analyzed by Basic Local Alignment Search Tool (BLAST, bioinformatics tool on NCBI website), the results revealed that multiple *Chlamydia* species were present in the *Borrelia*-infected BL skin tissues. In some of the BL tissues (4 out 6 samples), we were able to identify a common sequence with 99% identity to *C. pneumoniae* (KC512913; 98% coverage with E value: 7e-151), 86% identity to *C. psittaci* (KM247620; in 64% coverage with E value: 1e-61), and 76% to *C. trachomatis* (EU040365, in 71% of coverage and E value: 1e-40). The sequences were further analyzed by Clustal Omega multiple sequence alignment tool on the EMBL-EBI server (https://www.ebi.ac.uk/Tools/msa/clustalo/). Figure 1A shows a representative multiple sequence alignment of the BL *Chlamydia* OmpA sequence to the pathogenic *Chlamydia* sequences.

Using another published OmpA PCR protocol [69], we amplified a significantly different common sequence in some of the BL tissue samples (2 out 6 samples), showing 97% identity to *C. trachomatis* (JX559522; 93% coverage with E value 9e-50), 81% to *C. psittaci* (HM214490, in 67% of coverage

A

```
Chlamydia psittaci      CTTAAACATTTGGGATCGCTTCGACATTTTCTGCACCTTAGGGGCATCCAATGGATACTTCAA-AGCAAGTTCGG 75
Chlamydia trachomatis   ATTAAATATCTGGGATCGTTTTGATGTATTTTGTACATTGGGAGCAACTACCGGTTATTTAAA-AGGAAACTCTG 75
Chlamydia pneumoniae    CTTAAACATTTGGGATCGCTTTGATGTTTTCTGTACTTTAGGAGCTTCTAATGGTTACATTAG-AGGAAACTCTA 75
Chlamydia spp BL        TAGAGACACTCTGCATCG-TGTAATGCTTATTGTAGGCCGGGTTAGGTCTAT--CTACGGCAGTAGTATAGTTTG 75
                           * * *    * **** *   *    *  ** *     **             **    *  ** *   *

Chlamydia psittaci      CTGCATTCAACTTGGTTGGGTTAATAGGGTTTTCAGCTGCAAGCTCAATCTCTACCGATCTTCCAACGCAACTTC 150
Chlamydia trachomatis   CTTCCTTCAACTTAGTTGGATTATTCGGAACAAAAACACAATCTTCTAGCTTTA---ATACAGCGAAGCTTATTC 150
Chlamydia pneumoniae    CAGCGTTCAATCTCGTTGGTTTATTCGGAGTTAAAG------GTACTA-CTGTA-----AATGCAAATGAACTAC 150
Chlamydia spp BL        CAGCAGCGGATCCAGTAGGCTTGGCTCCCATAGAAA----ATGTTTTAGGTGCATCTACTTTTAAGATACGGTCG 150
                        *  *     *    ** ** **            *           *  *  *                    *

Chlamydia psittaci      CTAACGTAGGCATTACCCAAGGTGTTGTGGAATTTTATACAGACACATC---ATTTTCTTGGAGCGTAGGTG-CA 225
Chlamydia trachomatis   CTAACACTGCTTTGAATGAAGCTGTGGTTGAGCTTTATATAAACACTAC---CTTTGCTTGGAGCGTAGGTG-CT 225
Chlamydia pneumoniae    CAAACGTTTCTTTAAGTAACGGAGTTGTTGAACTTTACACAGACACCTC---TTTCTCTTGGAGCGTAGGCG-CT 225
Chlamydia spp BL        AAAACATAGTCTCCGTAAAATCCAGCACGTAAGCTAATAGCGTCGCACCAAGTAGCGCAAGGATCGCAAGGATCT 225
                          ***           *          *   * * *    * *  *        *  *** ** * *   *

Chlamydia psittaci      CGTGGAGCTTTATGGGAATGTGGTTGTGCAACTTTAGGAGCTGAGTTCCAATACGCTCAATCTAATCCTAAGATT 300
Chlamydia trachomatis   CGTGCAGCTCTCTGGGAATGTGGGTGTGCAACGTTAGGAGCTTCTTTCCAATATGCTCAATCTAAACCTAAAGTA 300
Chlamydia pneumoniae    CGTGGAGCCTTATGGGAATGCGGTTGTGCAACTTTGGGAGCTGAATTCCAATATGCACAGTCCAAACCTAAAGTT 300
Chlamydia spp BL        CCTGCAGCACCTTCCCA-TATTGTACCATCAATTAATAAGCTTGGATCAGAAGGGTTCCCTACAGGCAAGGCTTT 300
                        * ** ***    *   * *   *       *  *    ****    **  *   *  *  *  *  *      *

Chlamydia psittaci      GAAATGCT 308
Chlamydia trachomatis   GAAGAGTT 308
Chlamydia pneumoniae    GAAGAACT 308
Chlamydia spp BL        GTAAGGAG 308
                        * *
```

B

```
Chlamydia spp BL        GATCGACTGATTCTGTGGGAGGTTTCGGCGGAGATCCTTGCGATCCTTGCACCACTTGGT 60
Chlamydia trachomatis   TCGACGGAATTCTGTGGGAAGGTTTCGGCGGAGATCCTTGCGATCCTTGCACCACTTGGT 60
Chlamydia psittaci      TCGATGGCACTATGTGGGAAGGTGCTTCAGGAGATCCTTGCGATCCTTGCGCTACTTGGT 60
Chlamydia pneumoniae    TTGATGGTACAATATGGGAAGGTGCTGCAGGAGATCCTTGCGATCCTTGCGCTACTTGGT 60
                                    ** ****      ********************** * *******

Chlamydia spp BL        GTGACGCTATCAGCATGCGTATGGGTTACTATGGTGACTTTGTTTTCGACAACACAAC 118
Chlamydia trachomatis   GTGACGCTATCAGCATGCGTATGGGTTACTATGGTGACTTTGTTTTCGACCGTGTTTT 118
Chlamydia psittaci      GTGACACCATTAGCATCCGCGCAGGATACTACGGAGATTATGTTTTCGATCGTGTATT 118
Chlamydia pneumoniae    GCGACGCTATTAGCTTACGTGCTGGATTTTACGGAGACTATGTTTTCGACCGTATCTT 118
                        * *** * ** *** * * **    ** *  ** ** ** * *********
```

Figure 1. (A) A multiple sequence alignment obtained from Clustal Omega analyses representing BL *Chlamydia* OmpA DNA sequence mapped against different *Chlamydia* strains of *Chlamydia psittaci* (KM247620), *Chlamydia trachomatis* (EU040365), and *Chlamydia pneumoniae* (KC512913). (B) Clustel Omega multiple sequence alignment of OmpA gene DNA sequences obtained from BL tissues against different *Chlamydia* strains such as *Chlamydia trachomatis* (JX559522), *Chlamydia psittaci* (HM214490), and *Chlamydia pneumoniae* (DQ358972). Asterisks represent identical nucleotide sequence in all four *Chlamydia* sequences

and E value 2e-19), and 79% identity to *C. pneumoniae* (DQ358972; in 80% coverage with E value 2e-20).

Figure 1B shows a multiple sequence alignment obtained from Clustal Omega EMBI/EBI server representing DNA sequences from BL tissue OmpA DNA samples mapped against 3 strains of *Chlamydia trachomatis* (JX559522), *Chlamydia psittaci* (HM214490), and *Chlamydia pneumoniae* (DQ358972).

***Immunohistochemical (IHC) Staining of Human Biopsy Skin Tissues for Borrelia* and *Chlamydia*.** To further prove the presence of *Chlamydia* species and to determine whether there is a potential co-existence of the previously identified *Borrelia* biofilms found in these BL biopsy tissues [21], IHC staining techniques were used which were specific for *Borrelia*, *Chlamydia*, and alginate (biofilm marker) antigens.

Figure 2 shows that positive immunostaining for *Borrelia* (Figure 2, panels A, F, and K, green arrows,) and for the biofilm-specific marker alginate (Figure 2, panels C, H, and M, blue arrows) is present in all 6 BL biopsy tissues. For some tissue sections, the *Borrelia*–alginate positive aggregates also showed positive co-staining for *Chlamydia* spp. (Figure 2, Panels B and G, red arrows); however, some of the tissue sections only stained positive for *Borrelia* and alginate (Figure 2, panels K and M) but not for *Chlamydia* (Figure 2, panel L). Crucially, there was no immunostaining for *Chlamydia* spp. in the biofilm-free regions of tissues; however, *Borrelia* spirochetes were found frequently in the vicinity of the biofilm structures (Figure 2, panels A, F, and K green arrowheads). As reported previously [21, 22], those spirochetes were all negative for alginate antibody [Figure 2, panels C, H, and M].

All of the IHC experiments included 2 independent negative controls to prove the specificity of antibodies: non-specific IgG antibody and normal human skin samples. No signal was observed in the BL skin tissues when non-specific antibody was used in the IHC procedure (Figure 2, panels D, I, N, S, and Y). Furthermore, there were no immunostaining on the 20 commercially purchased human foreskin (Figure 2, panels P, Q, R, S, and T) and 20 healthy skin tissue sections (Figure 2, panels V, W, X, Y. and Z) for *Borrelia* and *Chlamydia*, as well as alginate antigens. To demonstrate the structure of the biofilm and how it is embedded in the tissue, the morphology of the BL skin tissues was visualized using a differential interference contrast microscopy method (DIC; Figure 2, panels E, J, O, T, and Z).

All images are taken with relatively low magnification (200×) to demonstrate the biofilm surrounding tissues and to show the background signals of the IHC methods.

To further analyze and understand the frequency of co-existence of *Chlamydia* spp. in *Borrelia* biofilms, an additional 150 sections were stained using IHC staining procedures described above. Figure 3 shows representative images of *Borrelia*/alginate and *Chlamydia*-positive staining biofilms; a higher magnification (400×) is used than that used in Figure 2 for a better visualization of their structures. *Borrelia*-positive aggregates were seen in all BL skin tissue samples (Figure 3, panels A, E, I, M, and R, green arrows, ref). Those structures were also stained positive for alginate, showing that they are indeed biofilms (Figure 3, panels C, G, K, O, and T, blue arrows). Most *Borrelia* and alginate positive structures stained positive for *Chlamydia* (Figure 3, panels B and F, red arrows). However, not all of those biofilm structures were positive for *Chlamydia* which further shows the specificity of our IHC protocol, (Figure 3, panels J, N, and S). The differential interference images depict the tissue morphology and the structure of the biofilm (Figure 3, panels D, H, L, P, and V).

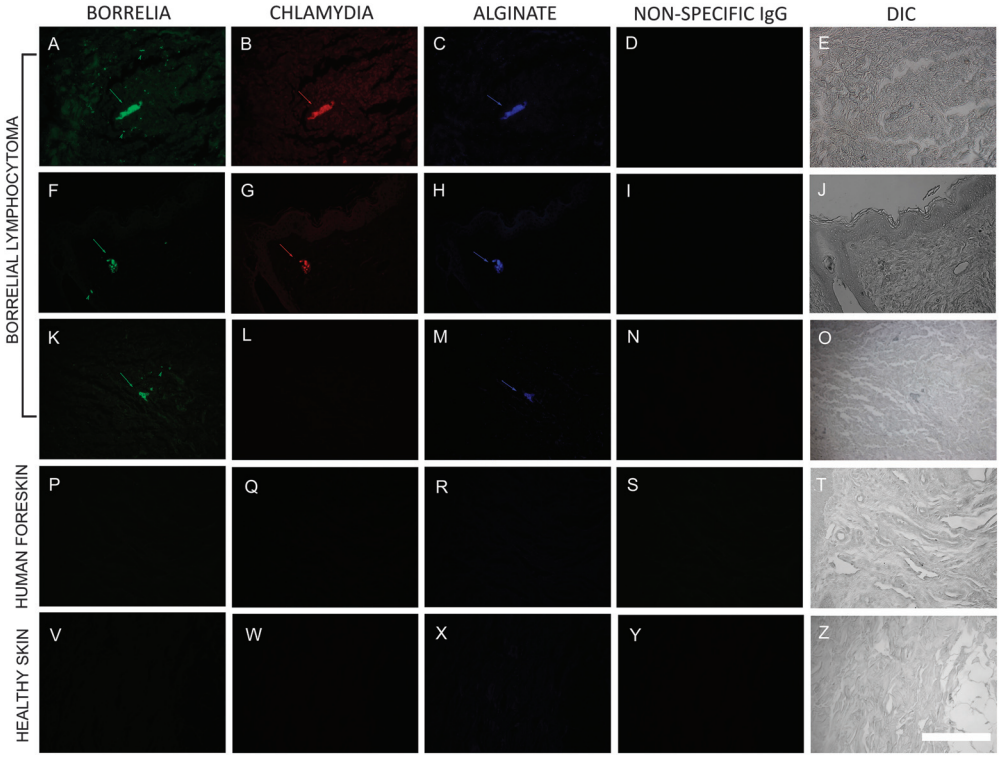

Figure 2. Representative IHC images of *Borrelia*, *Chlamydia*, and alginate staining in *Borrelia*-infected BL skin tissues. Panels A, F, K, P, and V show IHC staining results of skin tissues using a FITC labeled anti-*Borrelia* antibody (green arrows and arrowheads). Panels B, G, L, Q, and W show staining results with anti-chlamydia antibody (red arrows). Panels C, H, M, R, and X show staining of anti-alginate antibody (blue arrows). Panels D, I, N, S, and Y show results of staining with non-specific IgG antibody. Panels E, J, O, T, and Z are the differential interference contrast (DIC) images that show the morphology of the tissues. Panels A–O corresponds to BL skin tissues while panels P–T include negative controls corresponding to skin tissues from healthy human foreskin, and panels V–Z include negative controls corresponding to healthy skin tissues. All images were taken at 200× magnification. Scale bar: 200 μm

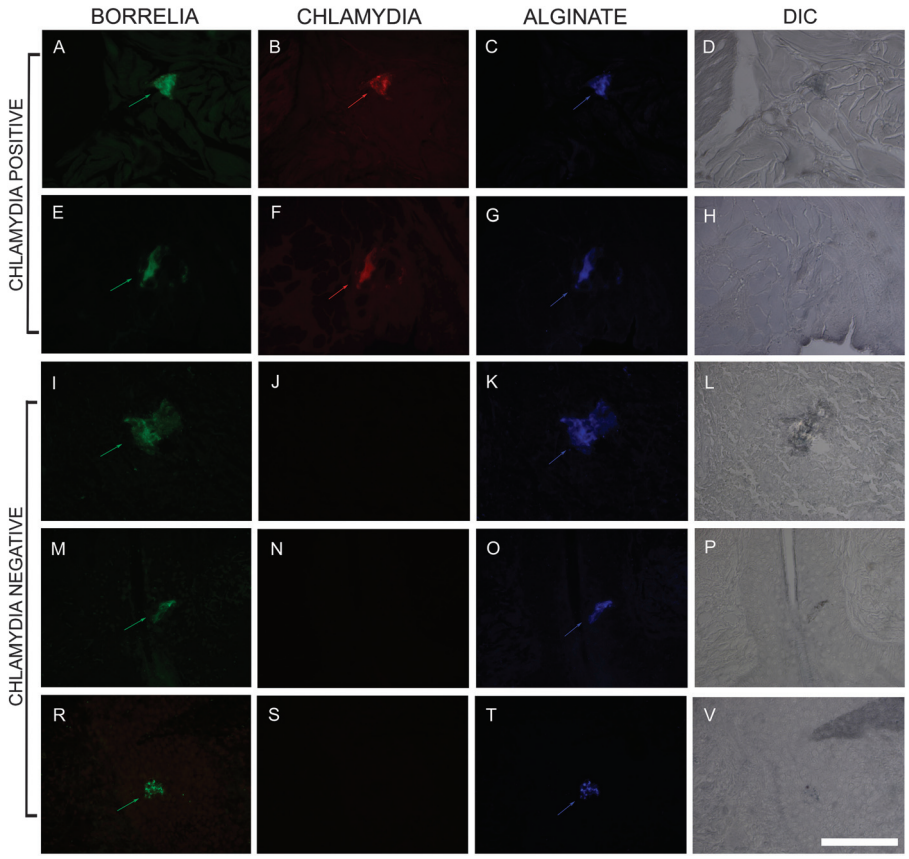

Figure 3. Representative images of IHC staining of BL biopsy skin tissues with *Borrelia*, *Chlamydia,* and alginate-specific antibodies. Panels A, E, I, M, and R show IHC positive staining for *Borrelia* (green arrows), and panels B and F show positive staining of *Chlamydia* (red arrows), while panels J, N, and S show negative staining for *Chlamydia* spp. Panel C, G, K, O, and T depict positive staining for alginate (blue arrows). Panel D, H, L, P, and V show DIC images. All images were taken at 400× magnification. Scale Bar: 200 μm

Quantitative analysis of a total of 150 IHC stained slides was carried out to categorize the size and frequency of the co-localization of *Borrelia* biofilms with *Chlamydia* spp. in BL skin tissues by direct counting of the positive structures. Each slide contained 2–4 biofilms and each biofilm size varied from a range of 20–80 μm.

Approximately 84% of *Borrelia* positive biofilms were positive for co-existence with *Chlamydia* spp. (Figure 4).

***FISH Staining of Human Biopsy Skin Tissues for Borrelia* and *Chlamydia*.** To further confirm the results obtained by IHC staining, fluorescent in situ hybridization (FISH) methods were utilized. FISH probes specific for 16S rDNA of *Borrelia* and *Chlamydia* were chosen from previously validated studies [21, 70]. For each slide containing structures, IHC-positive for *Borrelia* (green staining, Figure 5, panel A) that co-stained with *Chlamydia* spp. antibody (red staining, Figure 5, panel B) and with the biofilm marker alginate (blue staining, Figure 5, panel C), the next consecutive slide was stained using a combined IHC and FISH technique. The *Borrelia*-species-specific 16S rDNA probe (green staining, Figure 5, Panel E) was co-localized with the *Chlamydia*-DNA-specific 16S rDNA probe (red staining, Figure 5, panel F). The *Borrelia*/*Chlamydia*-positive structures also stained positive for IHC staining using anti-alginate antibody which confirmed the co-localization of *Borrelia* biofilms with *Chlamydia* spp. in the BL skin tissues. Several negative controls were included in the study to confirm the specificity of the chosen FISH probes with our target organisms. Competing oligonucleotide probes showed no significant staining for both *Borrelia* (Figure 5, panel I) and *Chlamydia* (Figure 5, panel J). As additional negative controls, a random DNA probe (Figure 5, panel K) and a DNAse I pre-treated sample (Figure 5, panel L) were used which resulted in no significant staining. The tissue morphology was visualized using the DIC images, which show how the biofilm is embedded in the tissue (Figure 5, panels D and H).

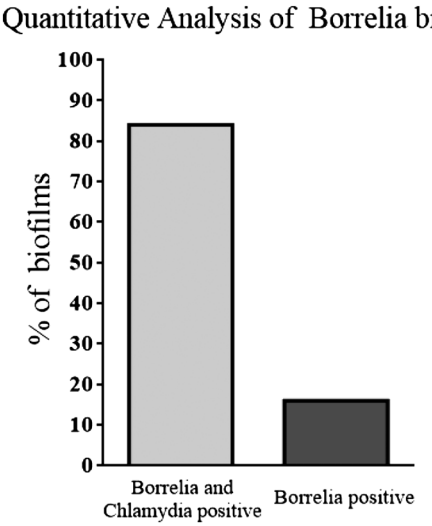

Figure 4. Quantitative analysis of *Borrelia* biofilms for positive *Borrelia* and *Chlamydia* IHC staining

***Confocal Imaging of Borrelia* and *Chlamydia* Positive Tissues.** A tissue section that was IHC positive for co-existence of *Borrelia* and *Chlamydia* and for the biofilm marker alginate (Figure 6, panels A, B, and C) were scanned with a confocal scanning laser microscope (Leica DMI6000) to further analyze the structure of the biofilm in the BL skin tissues

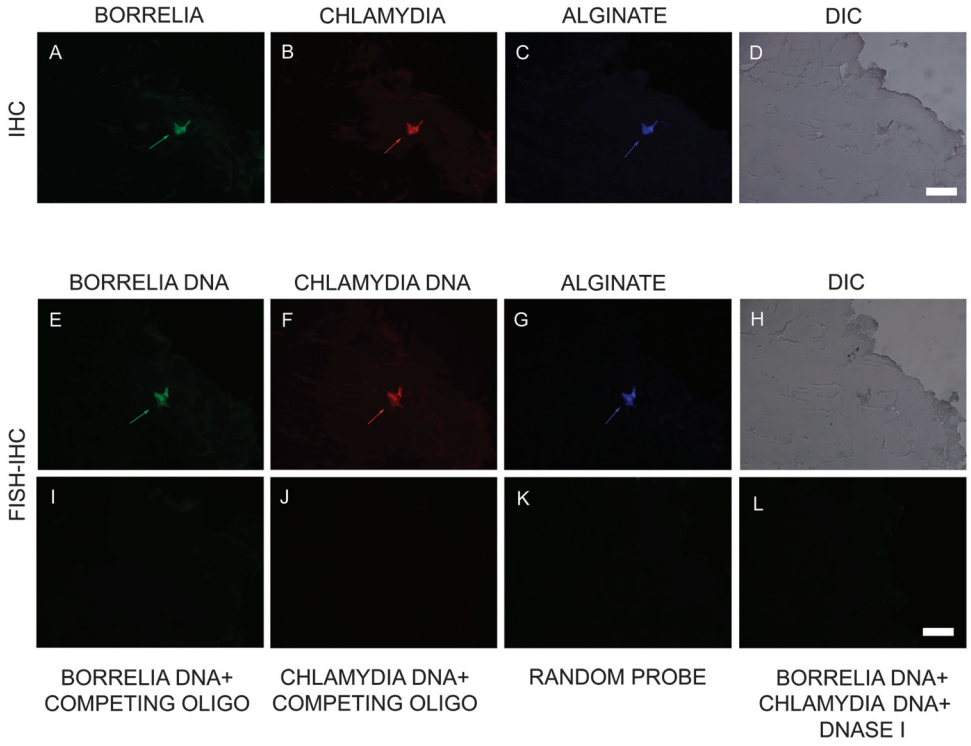

Figure 5. Representative images of the IHC staining on BL skin tissue section and the images of the consecutive slides stained with combined fluorescent in situ hybridization (FISH) and IHC techniques. Panels A, B, and C are the results of skin tissues stained with antibodies against *Borrelia* (green arrow), *Chlamydia* (red arrow), and alginate (blue arrow), respectively. Panels E and I show the staining results of skin tissues with 16S rDNA probe for *Borrelia burgdorferi* (green arrow). Panels F and J show the staining results of skin tissues with 16S rDNA probe for *Chlamydia* spp. (red arrow). Panel G is stained with antibodies for alginate (blue arrow). Panels D and H depict the morphology of the skin tissues using DIC microscopy methods. As comprehensive negative controls, a competing oligonucleotide (panels I and J for *Borrelia* and *Chlamydia*, respectively), a random DNA probe (panel K), and a DNase-treated samples (panel L) were used on consecutive tissue sections to further show the specific city of the 16S rDNA probe (for further details of the experimental conditions can be in Materials and Methods). All images were taken at 400× magnification. Scale bar: 100 μm

in a three-dimensional view. The obtained image shows the spatial distribution and the integrity of the biofilm along with the individual Z stacks further providing evidence for *Borrelia* and *Chlamydia* co-existence in the *Borrelia*/alginate positive structure (Figure 6, panel E, F, and G). The individual Z stacks show aggregates of *Chlamydia* enclosed within the center of *Borrelia* biofilm (Figure 6, panel F, red arrows). The individual Z stacks of *Borrelia* and alginate show how alginate, a component of the EPS layer, surrounds the *Borrelia* biofilm (Figure 6, panel G, blue arrow).

Discussion

Previous studies have shown that *Borrelia burgdorferi* sensu stricto and the sensu lato group are capable of forming biofilms in vitro [19, 20]. Recently, we also provided in vivo evidence for the presence of *Borrelia burgdorferi* biofilms in

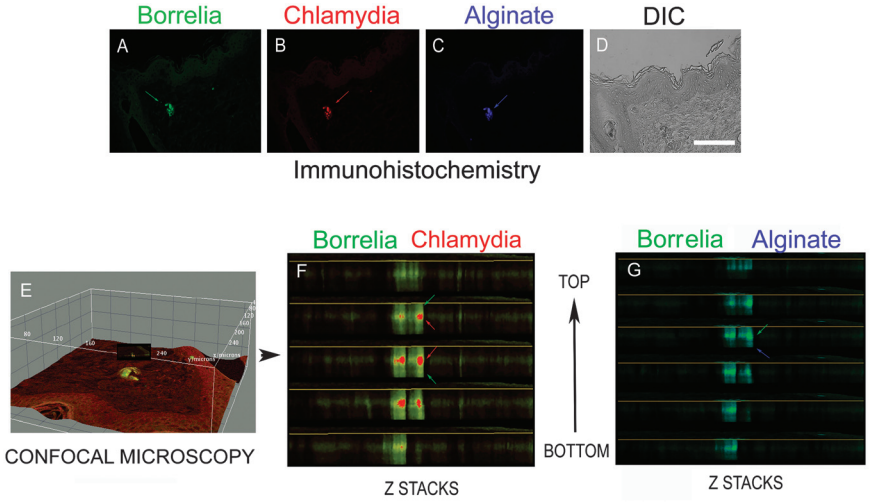

Figure 6. Three-dimensional (3D) analyses of *Borrelia* and *Chlamydia* mixed biofilm in human BL skin biopsy tissue using confocal microscopy. Panels A, B, and C are the results of skin tissues positively immunostained with antibodies against *Borrelia* (green arrow), *Chlamydia* (red arrow), and alginate (blue arrow), respectively. Panel D shows the DIC image to depict the morphology of the tissue. Confocal microscopy shows the 3D distribution of mixed biofilms and the individual Z stacks focus on the biofilms showing *Borrelia* and *Chlamydia* (panel F) and *Borrelia* and alginate (panel G) spatial distribution. Scale bar: 100 μm

Borrelia-infected skin lesions called *Borrelia* lymphocytoma (BL) [21]. However, the question of co-existence of *Borrelia* biofilms in the multi-species form is yet to be answered. This study investigated the presence of potential co-infections of *Borrelia* biofilms with *Chlamydia* spp. It is among the first to document the co-existence of *Borrelia* biofilms with the intracellular pathogen *Chlamydia* spp. in infected human skin tissues, and to the best of our knowledge, this is the first study to show *Chlamydia* within the biofilm.

Our PCR and sequencing analyses showed that *Borrelia* positive BL tissue samples are also positive for *Chlamydia* DNA, and the obtained sequencing was mapped to several chlamydial strains and was found to have the best match to 2 human pathogens, *C. pneumoniae* and *C. trachomatis* strains. Studies conducted in Finland and Australia reported *Chlamydia*-like DNA in skin biopsies of patients suspected to have a tick bite and who were PCR-positive for *Borrelia* DNA as well [50–52]. A very recent study provided evidence that IgM and IgG antibodies for both *C. pneumoniae* and *C. trachomatis* can be detected in 20–30% of patients with tick bite history [71]. Those studies strongly indicated that co-infection of *Borrelia* with *Chlamydia* spp. is possible.

After finding chlamydial DNA in BL skin biopsies, the question became whether they exist in biofilm form. To examine BL skin lesions for co-existence of *Borrelia* and *Chlamydia* in biofilm form, IHC staining and FISH techniques were used.

As previously reported, alginate is successfully being adapted as a biofilm marker and was used to confirm the co-existence of both bacterial species in the biofilm form [19]. Alginate has been reported to be a key component of the EPS layer in *Borrelia burgdorferi* sensu stricto and sensu lato biofilms [19–21]. Although no direct evidence suggests the existence of *Chlamydia* individually in a biofilm form, they could be a part of a microbial community with other bacterial biofilms. Biofilm forming bacteria can promote the participation of strains of non-biofilm forming bacteria in a community as is observed in dental plaques with *Actinomycetes* spp. [72].

In fact, our IHC and FISH data suggest that *Chlamydia* spp. can exist in aggregate forms as suggested on other systems [60, 66]. Furthermore, environmental stressors are known to push *Chlamydia* into a state of persistence, in which they are viable but non-infectious [73]. Persistent like morphological characteristics of *Chlamydia* have been identified in vivo [74] and several studies have shown resistance of chlamydial infection to antibiotics both in vitro and in vivo [75].

Our confocal microscopy data suggest a very specific spatial distribution of *Chlamydia* in the *Borrelia* biofilm. Previous studies suggested that the different bacteria in multi-species biofilms could have specific spatial distribution which supports our confocal image findings showing that *Chlamydia* is localized in the middle of *Borrelia* biofilm rather than randomly distributed [42, 77, 78]. Our confocal analyses also demonstrated that the *Borrelia*/*Chlamydia*-positive biofilm structure is surrounded by alginate. The observation raises the question about which organism secretes alginate rich protective matrix. While studies show that *Chlamydiae*-infected cell cultures express a glycolipid that is similar to alginate in its polysaccharide content and molecular weight [76], our data suggests that the alginate being expressed is probably secreted by *Borrelia burgdorferi* and not by *Chlamydia* because all *Chlamydia* negative biofilms are positive for alginate.

Ticks are capable of inoculating and harvesting several different pathogens upon infection to the host organism. A study conducted in Switzerland and Algeria evaluated ticks and fleas for the presence of *Chlamydiales* DNA and found ticks to be a possible vector for transmission of *Chlamydia* spp. [50]. The same group in 2015 then reported a higher prevalence and diversity of *Chlamydiales* DNA in ticks [51]. Another study supported and confirmed the presence of *Chlamydia*-related organism in ticks [52], and they also found sequences similar to *Chlamydia* DNA in human skin biopsies. The study screened skin biopsies of patients with suspected history of tick bite and reported *Chlamydia* DNA in 85% *Borrelia* PCR positive biopsies and 71% positive for *Chlamydia* DNA in *Borrelia* PCR negative skin biopsies [52].

Mono-species biofilms alone have proven to be 100 to 1000 times more resistant to antibiotics, leading to persistent infections [79]. Our research group has demonstrated the extraordinary resistance of *Borrelia* biofilms to several antibiotics in vitro [22, 80], which may explain the persisting symptoms observed in Lyme patients. Multi-species biofilms are being studied extensively in relation to several chronic infections. Chronic wound infections in a porcine model showed increased resistance to antimicrobial activity upon infection with *Staphylococcus aureus* in a multi-species biofilm form [39, 81, 82]. Pulmonary infections in cystic fibrosis patients have been suggested to contain several different airway pathogens making them more complex and resistant to treatments [40]. Studies have identified *Dolosigranulum pigrum* and *Pseudomonas aeruginosa* in biofilm form in pulmonary infections and have shown increased resistance to antimicrobial treatments [40]. Diabetic foot ulcers show polymicrobial infection involving *S. aureus*, *P. aeruginosa*, and *E. coli* at the site of infection, slowing the healing process and, in some cases, leading to antimicrobial resistance [83]. These findings strongly suggest that microbial communities behave synergistically with each other in a mixed biofilm form.

The symptoms observed during Lyme infection are very similar to those of chlamydial infection [62, 63]. Arthritis is one of the major symptoms observed in both of these bacterial infections, and a study suggested the intra-articular co-infection of *Chlamydia trachomatis* and *Borrelia burgdorferi* in patients with oligoarthritis [63]. Furthermore, *Chlamydia* and *Borrelia* DNAs were found in the synovial fluid of patients with undifferentiated oligoarthritis [84].

Another example for skin infections, which can be caused by *Borrelia* or *Chlamydia*, is erythema nodosum, a condition leading to skin inflammation with painful, red deep-seated nodules [62, 85]. The skin condition erythema multiforme has been also associated with *Borrelia* and *C. pneumoniae* infections [86, 87].

Furthermore, *C. pneumonia* infections have been linked to atherosclerosis and well characterized in atherosclerotic plaques [58]. Lyme carditis is one of the chronic infections of Lyme disease, and an independent study reported seropositivity results for anti-*Borrelia* IgG antibodies in carotid atherosclerosis [88]. In addition, a recent study observed biofilm formation in atherosclerotic plaques, which indeed suggests that biofilms could be present in cardiac tissues and be a part of the biofilm community with several other species [89, 90].

The obvious question is whether multi-species biofilms could have even higher antibiotic resistance for antibiotics than mono-species biofilm. In a synergistic relationship, both biofilm partners should provide advantage for the whole community [42]. The obvious question is why *Borrelia* and *Chlamydia* can be found together so frequently and how they can build symbiotic relationships. *Chlamydia*, for example, cannot produce the ATP molecule for its energetic processes [58–61]. Therefore, it is possible that *Borrelia* must provide ATP inside the biofilm structure. Furthermore, *Borrelia* biofilm is known to have a very organized structure that confers high resistance to environmental stressors [19, 20, 21]; therefore, *Borrelia* could also provide the necessary shelter for *Chlamydia*.

Conversely, *Chlamydia* could supply iron necessary for *Borrelia*. Several studies have reported that *Borrelia* uses manganese instead of iron for its own biological processes [91, 92]. Yet, iron appears to play a crucial role in biofilm formation by stabilizing the polysaccharide matrix, as was shown in *S. aureus* and *P. aeruginosa* biofilms [93–95]. Moreover, in a multi-species biofilm of *Candida albicans* and *P. aeruginosa*, iron triggers virulence of the bacterial pathogens and can cause significant damage to the host [96]. Relating the role of *Chlamydia* in the biofilm form with *Borrelia* could suggest that they have a symbiotic relation.

In summary, our data provides strong evidence for the co-existence of *Chlamydia* spp. with *Borrelia* biofilms in human skin biopsies of BL lesions with their involvement in *Borrelia* biofilms. This study warrants further research to understand the physiological role of mixed biofilms in chronic Lyme disease.

Abbreviations

ATCC - American Type Culture Collection
BL - Borrelial lymphocytoma
BSA - bovine serum albumin
BSK-H - Barbour-Stoner-Kelly H
DIC - differential interference contract microscopy
EM - erythema migrans
EDTA - ethylenediaminetetraacetic acid
FAM - 6-fluorescein amidite
FFPE - formalin-fixed, paraffin-embedded
FISH - fluorescent in situ hybridization
FITC - fluorescein isothiocyanate
H&E - hematoxylin and eosin
IHC - immunohistochemistry
OmpA - major outer membrane protein A
PBS - phosphate-buffered saline
PCR - polymerase chain reaction
RT - room temperature
SSC - saline sodium citrate

Funding Sources

This work was supported by grants from the University of New Haven, National Philanthropic Trust, LivLyme Foundation, Lyme Warriors and CT Lyme Riders scholarships to KG and KW. We also thank the Schwartz Research foundation for the donation of the Leica DM2500 microscope, as well as the Hamamatsu ORCA Digital Camera.

Authors' Contribution

ES conceptualized, designed, and supervised the study, analyzed and interpreted data, obtained funding, and wrote the manuscript. KG designed and performed experiments, analyzed and interpreted data, and wrote manuscript. KW, JT, and GG designed and performed experiments. AM analyzed and interpreted data. BZ conceptualized and designed the study. All authors had full access to all data in the study and take responsibility for the integrity of the data and the accuracy of the data analysis.

Conflict of Interest

The authors have declared that no competing interest exists.

Acknowledgements. The authors would like to thank Dr. Gerald B. Pier (Harvard University) for the anti-alginate antibody. We also thank Dr. Dougles Brash and Dr. Joseph J. Burrascano for their helpful suggestions for the final manuscript.

References

1. Burgdorfer W, Barbour AG, Hayes SF, Benach JL, Grunwaldt E, Davis JP. Lyme disease-a tick-borne spirochetosis?. Science. 1982;216:1317–19.
2. Lane RS, Piesman J, Burgdorfer W. Lyme borreliosis: relation of its causative agent to its vectors and hosts in North America and Europe. Annu Rev Entomol. 1991;36:587–609.
3. Baranton G, Postic D, Saint Girons I, Piffarettiet JC, Assous M, Grimont PA. Delineation of *Borrelia burgdorferi* sensu stricto, *Borrelia garinii* sp. nov., and group VS461 associated with Lyme borreliosis. Int J Syst Bacteriol. 1992;42:378–83.
4. Steere AC, Coburn J, Glickstein L. The emergence of Lyme disease. J Clin Invest. 2004;113:1093–101.
5. Rudenko N, Golovchenko M, Grubhoffer L, Oliver JH. Updates on *Borrelia burgdorferi* sensu lato complex with respect to public health. Ticks Tick Borne Dis. 2011;2:123–8.
6. Mead PS. Epidemiology of Lyme Disease. Infect Dis Clin North Am. 2015;29:87–210.
7. Ackermann R, Kabatzki J, Boisten HP, Steere AC, Grodzicki L, Hartug S, Runne U. Ixodes ricinus spirochete and European erythema chronicum migrans disease. Yale J Biol Med. 1984;57:573–80.
8. Eisendle K, Zelger B. The expanding spectrum of cutaneous borreliosis. G Ital Dermatol Venereol. 2009;144:157–71.
9. Eisendle K, Grabner T, Zelger B. Focus floating microscopy: "Gold Standard" for cutaneous Borreliosis*?* Am J Clin Pathol. 2007;127:213–22.
10. Wormser GP. Clinical practice. Early Lyme disease. N Engl J Med. 2006;354:2794–801.
11. Müllegger RR, Glatz M. Skin manifestations of lyme borreliosis: diagnosis and management. Am J Clin Dermatol. 2008;9:355–68.
12. Kandhari R, Kandhari S, Jain S. Borrelial lymphocytoma cutis: a diagnostic dilemma. Indian J Dermatol. 2014;59:595–607.
13. Cary NR, Fox B, Wright DJ, Cutler SJ, Shapiro LM, Grace AA. Fatal Lyme carditis and endodermal heterotopia of the atrioventricular node. Postgrad Med J. 1990;66:134–6.
14. Hildenbrand P, Craven DE, Jones R, Nemeskal P. Lyme neuroborreliosis: manifestations of a rapidly emerging zoonosis. AJNR Am J Neuroradiol. 2009;30:1079–87.
15. Miklossy J. Chronic or late lyme neuroborreliosis: analysis of evidence compared to chronic or late neurosyphilis. Open Neurol J. 2012;6:146–57.
16. Scheffold N, Herkommer B, Kandolf R, May AE. Lyme carditis–diagnosis, treatment and prognosis. Dtsch Arztebl Int. 2015;112:202–8.
17. Smith BG, Cruz AI, Milewski MD, Shapiro ED. Lyme disease and the orthopaedic implications of lyme arthritis. J Am Acad Orthop Surg. 2011;19:91–100.
18. Lantos PM. Chronic Lyme disease. Infect Dis Clin North Am. 2015;29:325–40.
19. Sapi E, Bastian SL, Mpoy CM, Scott S, Rattelle A, Pabbati N, et al. Characterization of biofilm formation b*y Borrelia burgdorferi in vitro*. PLoS One. 2012;7:1–11.
20. Timmaraju VA, Theophilus PAS, Balasubramanian K, Shakih S, Luecke DF, Sapi E. Biofilm formation by *Borrelia sensu lato.* FEMS Microbiol Lett. 2015;362:fnv120. doi: 10.1093/femsle/fnv120.
21. Sapi E, Balasubramanian K, Poruri A, Maghsoudlou JS, Socarras KM, et al. Evidence of *in vivo* existence of *Borrelia* biofilm in Borrelial Lymphocytomas. Eur J Microbiol Immunol (Bp). 2016;6:9–24.
22. Sapi E, Kaur N, Anyanwu S, Datar A, Patel S, Rossi JM, et al. Evaluation of *in vitro* antibiotic susceptibility of different morphological forms of *Borrelia burgdorferi*. Infect Drug Resist. 2011;4:97–113.
23. Costerton JW, Stewart PS, Greenberg EP. Bacterial biofilms: a common cause of persistent infections. Science. 1999;284:1318–22.
24. Sutherland I. Biofilm exopolysaccharides: a strong and sticky framework. Microbiol. 2001;147:3–9.
25. Hall-Stoodley L, Costerton JW, Stoodley P. Bacterial biofilms: from the natural environment to infectious diseases. Nat Rev Microbiol. 2004;2:95–108.
26. Flemming HC, Neu TR, Wozniak DJ. The EPS matrix: the "house of biofilm cells". J Bacteriol. 2007;189:7945–7.
27. Jiao Y, Cody GD, Harding AK, Wilmes P, Schrenk M, et al. Characterization of extracellular polymeric substances from acidophilic microbial biofilms. Appl Environ Microbiol. 2010;76:2916–22.
28. Amato SM, Fazen CH, Henry TC, Mok WW, Orman MA, et al. The role of metabolism in bacterial persistence. Front Microbiol. 2014;5:70. doi: 10.3389/fmicb.2014.00070.
29. Conlon BP, Rowe SE, Lewis K. Persister cells in biofilm associated infections. Adv Exp Med Biol. 2015;831:1–9.
30. Lewis K, Shan Y. Why tolerance invites resistance. Science. 2017;355:96.
31. Lopes SP, Ceri H, Azevedo NF, Pereira MO. Antibiotic resistance of mixed biofilms in cystic fibrosis: impact of emerging microorganisms on treatment of infection. Int J Antimicrob Agents. 2012;40:260–3.
32. Sun F, Qu F, Ling Y, Mao P, Xia P, Chen H, Zhou D. Biofilm-associated infections: antibiotic resistance and novel therapeutic strategies. Future Microbiol. 2013;8:877–86.
33. Römling U, Balsalobre C. Biofilm infections, their resilience to therapy and innovative treatment strategies. J Intern Med. 2012;272:541–61.
34. Bjarnsholt T. The role of bacterial biofilms in chronic infections. APMIS Suppl. 2013;136:1–51.
35. Petersen NT, Høiby N, Mordhorst CH, Lind K, Flensborg EW, Bruun B. Respiratory infections in cystic fibrosis patients caused by virus, chlamydia and mycoplasma–possible synergism with *Pseudomonas aeruginosa*. Acta Paediatr Scand. 1981;70:623–8.
36. Fiedler T, Köller T, Kreikemeyer B. *Streptococcus pyogenes* biofilms-formation, biology, and clinical relevance. Front Cell Infect Microbiol. 2015;5:15. doi: 10.3389/fcimb.2015.00015.

37. Delcaru C, Alexandru I, Podgoreanu P, Grosu M, Stavropoulos E, Chifiriuc MC, Lazar V. Microbial biofilms in urinary tract infections and prostatitis: Etiology, pathogenicity, and combating strategies. Pathogens. 2016;5:65. doi:10.3390/pathogens5040065.

38. Wang J, Foxman B, Mody L, Snitkin ES. Network of microbial and antibiotic interactions drive colonization and infection with multidrug-resistant organisms. Proc Natl Acad Sci USA. 2017;14:10467–72. doi: 10.1073/pnas.1710235114.

39. Dalton T, Dowd SE, Wolcott RD, Sun Y, Watters C, Griswold JA, et al. An *in vivo* polymicrobial biofilm wound infection model to study interspecies interactions. PLoS ONE. 2011;6:e27317.

40. Lopes SP, Ceri H, Azevedo NF, Pereira MO. Antibiotic resistance of mixed biofilms in cystic fibrosis: impact of emerging microorganisms on treatment of infection. Int J Antimicrob Agents. 2012;40:260–3.

41. Burmølle M, Webb JS, Rao D, Hansen LH, Sørensen SJ, Kjelleberg S. Enhanced biofilm formation and increased resistance to antimicrobial agents and bacterial invasion are caused by synergistic interactions in multispecies biofilms. Appl Environ Microbiol. 2006;72:3916–23.

42. Elias S, Banin E. Multi-species biofilms: living with friendly neighbors. FEMS Microbiol Rev. 2012; 36(5):990-1004.

43. Brown JS: Oral biofilms, periodontitis and pulmonary infections. Oral Dis. 2007;13:513–4.

44. Burmølle M, Ren D, Bjarnsholt T, Sørensen SJ. Interactions in multispecies biofilms: do they actually matter? Trends Microbiol. 2014;22:84–91.

45. Berghoff W. Chronic Lyme disease and co-infections: Differential diagnosis. Open Neurol J. 2012;6:158–78.

46. Caulfield AJ, Pritt BS. Lyme disease coinfections in the United States. Clin Lab Med. 2015;35:827–46.

47. Diuk-Wasser MA, Vannier E, Krause PJ. Coinfection by Ixodes tick-borne pathogens: Ecological, epidemiological, and clinical consequences. Trends Parasitol. 2016;32:30–42.

48. Moutailler S, Valiente Moro C, Vaumourin E, Michelet L, Tran FH, Devillers E, et al. Co-infection of ticks: The rule rather than the exception. PLoS Negl Trop Dis. 2016;10:e0004539.

49. Raileanu C, Moutailler S, Pavel I, Porea D, Mihalca AD, Savuta G, Vayssier-Taussat M. *Borrelia* diversity and co-infection with other tick borne pathogens in ticks. Front Cell Infect Microbiol. 2017;7:36. doi:10.3389/fcimb.2017.00036.

50. Croxatto A, Rieille N, Kernif T, Bitam I, Aeby S, Peter O, Greub G. Presence of *Chlamydiales* DNA in ticks and fleas suggests that ticks are carriers of *Chlamydia*e. Ticks Tick Borne Dis. 2014;5:59–365.

51. Pilloux L, Aeby S, Gaümann R, Burri C, Beuret C, Greub G. The high prevalence and diversity of *Chlamydiales* DNA within Ixodes ricinus ticks suggest a role for ticks as reservoirs and vectors of *Chlamydia*-related bacteria. Appl Environ Microbiol. 2015;81:8177–82.

52. Hokynar K, Sormunen JJ, Vesterinen EJ, Partio EK, Lilley T, et al. *Chlamydia*-like organisms (CLOs) in Finnish *Ixodes ricinus* ticks and human skin. Microorg. 2016;4:28. doi: 10.3390/microorganisms4030028.

53. Tolkki L, Hokynar K, Meri S, Panelius M, Ranki A. Granuloma annulare and morphea: Correlation with *Borrelia burgdorferi* infections and *Chlamydia*-related bacteria. Acra Derma Venereol. 2018;98:355–60. doi: 10.2340/00015555-2831.

54. Burnard D, Weaver H, Gilett A, Loader J, Flanagan C, Polkinghome A. Novel *Chlamydiales* genotype identified in ticks from Australian wildlife. Paras Vec. 2017;10:46. doi: 10.1186/s13071-017-1994-y.

55. Stephens RS, Kalman S, Lammel C, Marathe R, Aravind L, et al. Genome sequence of an obligate intracellular pathogen of humans: *Chlamydia* trachomatis. Science. 1998;282:754–9.

56. Elwell C, Mirrashidi K, Engel J. *Chlamydia* cell biology and pathogenesis. Nat Rev Microbiol. 2016;14:385–400.

57. Fields KA, Hackstadt T. The chlamydial inclusion: escape from the endocytic pathway. Annu Rev Cell Dev Biol. 2002;18:221–45.

58. Belland RJ, Ouellette SP, Gieffers J, Byrne GI. *Chlamydia pneumoniae* and atherosclerosis. Cell Microbiol. 204;6:117–127. doi:10.1046/j.1462-5822.2003.00352.x.

59. Honarmand H. Atherosclerosis induced by *Chlamydophila pneumoniae*: A controversial theory. Interdiscip Perspect Infect Dis. 2013;2013:941392.

60. Clausen JD, Christiansen G, Holst HU, Birkelund S. *Chlamydia trachomatis* utilizes the host cell microtubule network during early events of infection. Mol Microbiol. 1997;25:44–449.

61. Michael RK, Konrad S. *Chlamydia psittaci*: update on an underestimated zoonotic agent. Pathogens and Dis. 2015;73:1–15.

62. Kousa M, Saikku P, Kanerva L. Erythema nodosum in chlamydial infections. Acta Derm Venereol. 1980;60:319–22.

63. Putschky N, Schnarr S, Wollenhaupt J, Zeidler H, Kuipers J. Intra-articular co-infection by *Borrelia burgdorferi* and *Chlamydia trachomatis*. Annals of the Rheumatic Diseases. 2001;60:632–4. doi:10.1136/ard.60.6.632.

64. Somani J, Bhullar VB, Workowski KA, Farshy CE, Black CM. Multiple drug-resistant *Chlamydia trachomatis* associated with clinical treatment failure. J Infect Dis. 2000;181:1421–7.

65. Yamaguchi H, Friedman H, Yamamoto M, Yasuda K, Yamamoto Y. *Chlamydia* pneumoniae resists antibiotics in lymphocytes. Antimicrob Agents Chemother. 2003;47:1972–5.

66. Majeed M, Gustafsson M, Kihlström E, Stendahl O. Roles of Ca2+ and F-actin in intracellular aggregation of *Chlamydia trachomatis* in eukaryotic cells. Infect Immun. 1993;61:1406–14.

67. Majeed M, Krause KH, Clark RA, Kihlström E, Stendahl O. Localization of intracellular Ca2+ stores in HeLa cells during infection with *Chlamydia trachomatis.* J Cell Sci. 1999;112:35–44.

68. Sabagh F, Storey CC. The development of polymerase chain reaction (PCR) to detect *C. pneumoniae* and *C. psittaci.* J Paramed Sci (JPS). 2010;1:43–52.

69. Rostami NM, Rashidi HB, Aghsaghloo F, Nazari R. Comparison of clinical performance of antigen based-enzyme immunoassay (EIA) and major outer membrane protein (MOMP)-PCR for detection of genital *Chlamydia* trachomatis infection. Int J Reprod Biomed (Yazd). 2016;14:411–20.

70. Poppert S, Essig A, Marre R, Wagner M, Horn M. Detection and differentiation of chlamydiae by fluorescence *in situ* hybridization. Appl Environ Microbiol. 2002;68:4081–9.

71. Garg K, Meriläinen L, Franz O, Pirttinen H, Quevedo-Diaz M, Croucher S, Gilbert L. Evaluating polymicrobial immune responses in patients suffering from tick-borne diseases. Sci Rep. 2018;8:15932. doi:10.1038/s41598-018-34393-9.

72. Filoche SK, Anderson SA, Sissons CH. Biofilm growth of Lactobacillus species is promoted by Actinomyces species and Streptococcus mutans. Oral Microbiol Immunol. 2004;19:322–6.

73. Borel N, Pospischil A, Hudson AP, Rupp J, Schoborg RV. The role of viable but non-infectious developmental forms in chlamydial biology. Front Cell Infect Microbiol. 2014;4:97.

74. Phillips Campbell R, Kintner J, Whittimore J, Schoborg RV. *Chlamydia muridarum* enters a viable but non-infectious state in amoxicillin-treated BALB/c mice. Microbes Infect. 2012;14:1177–85.

75. Sandoz KM, Rockey DD. Antibiotic resistance in *Chlamydia*e. Future Microbiol. 2010;5:1427-1442.

76. Tolker-Nielsen T, Molin S. Spatial organization of microbial biofilm communities. Microb Ecol. 2000;40:75–84.

77. Stuart ES, Tirrell SM, MacDonald AB. Characterization of an antigen secreted by *Chlamydia*-infected cell culture. Immunol. 1987;61:527–33.

78. Mitri S, Xavier JB, Foster KR. Social evolution in multispecies biofilms. Proc Natl Acad Sci USA. 2011;108:10839–46.

79. Stewart PS, Costerton JW. Antibiotic resistance of bacteria in biofilms. Lancet. 2001;358:135–8.

80. Theophilus PA, Victoria MJ, Socarras KM, Filsuh KR, Gupta K, Luecke DF: Effectiveness of stevia rebaudiana whole leaf extract against the various morphological forms of *Borrelia burgdorferi in vitro.* Eur J Microbiol Immunol (Bp). 2015;5:268–80.

81. Davis SC, Ricotti C, Cazzaniga A, Welsh E, Eaglstein WH, Mertz PM. Microscopic and physiologic evidence for biofilm-associated wound colonization *in vivo*. Wound Repair Regen. 2008;16:23–9.

82. Hotterbeekx A, Kumar-Singh S, Goossens H, Malhotra-Kumar S. *In vivo* and *in vitro* interactions between *Pseudomonas aeruginosa* and *Staphylococcus spp*. Front Cell Infect Microbiol. 2017;7:106. doi:10.3389/fcimb.2017.00106.

83. Shanmugam PMJ, Susan SL. The bacteriology of diabetic foot ulcers, with a special reference to multidrug resistant strains. J Clin Diagn Res. 2013;7:441–5.

84. Schnarr S, Putschky N, Jendro MC, Zeidler H, Hammar M, Kulpers JG, Wollenhaupt J. *Chlamydia* and *Borrelia* DNA in synovial fluid of patients with early undifferentiated oligoarthritis: results of a prospective study. Arthritis Rheum. 2001;44:2679–85.

85. Simakova AL, Popov AF, Dadalova OB. Ixodes tick-borne borreliosis with erythema nodosum. Med Parazitol (Mosk). 2005;4:31–2.

86. Hosokawa R, Kobayashi T, Higashino T, Asano C, Ono K, Fijimoto N, Tajima S. Two cases of erythema exsudativum multiforme associated with *Chlamydia pneumoniae* infection. J Dermatol. 2012;39:306–8.

87. Imashuku S, Kudo N. *Chlamydia pneumoniae* infection-associated erythema multiforme. Pediatr Rep. 2013;5:35–7. doi: 10.4081/pr.2013.e9.

88. Völzke H, Wolff B, Lüdemann J, Guertler L, Kramer A, John U, Felix SB. Seropositivity for anti-*Borrelia* IgG antibody is independently associated with carotid atherosclerosis. Atherosclerosis. 2016;184:108–12.

89. Allen HB, Boles J, Morales D, Ballal S, Joshi SG. Arteriosclerosis: The novel finding of biofilms and innate immune system activity within the plaques. J Med Surg Pathol. 2016;1:135.

90. Kang SG, Chung WC, Song SW, Joo KR, Lee H, Kang D, Lee JS, Lee KM. Risk of artherosclerosis and *Helicobacter pylori* infection according to CD14 promotor polymorphism in healthy Korean population. Gastroenterol Res Pract. 2013; 2013:570597.

91. Posey JE, Gherardini FC. Lack of a role for iron in the Lyme disease pathogen. Science. 2000;288:1651–3.

92. Troxell B, Xu H, Yang XF. *Borrelia burgdorferi*, a pathogen that lacks iron, encodes manganese-dependent superoxide dismutase essential for resistance to streptonigrin. J Biol Chem. 2012;287:19284–93.

93. Berlutti F, Morea C, Battistoni A, Sarli S, Cipriani P, Superti F, Ammendolia MG, Valenti P. Iron availability influences aggregation, biofilm, adhesion and invasion of *Pseudomonas aeruginosa* and *Burkholderia cenocepacia*. Int J Immunopathol Pharmacol. 2005;18:661–70.

94. Lin MH, Shu JC, Huang HY, Cheng YC. Involvement of iron in biofilm formation by *Staphylococcus aureus*. PLoS One. 2012;7:e34388. doi: 10.1371/journal.pone.0034388.

95. Weinberg ED. Suppression of bacterial biofilm formation by iron limitation. Med Hypot. 2004;63:863–5.

96. Trejo-Hernández A, Andrade-Domínguez A, Hernández M, Encarnación S. Interspecies competition triggers virulence and mutability in *Candida albicans-Pseudomonas aeruginosa* mixed biofilms. ISME J. 2014;8:1974–88.